RSC Advances

PAPER

View Article Online
View Journal | View Issue

Cite this: *RSC Adv.*, 2024, **14**, 7112

Surface-enhanced Raman spectroscopy for studying the interaction of organometallic compound bis(1,3-dihexylimidazole-2-yl) silver(I) hexafluorophosphate (V) with the biofilm of *Escherichia coli*†

Tania Tabussam, ‡[a] Hina Shehnaz,‡[a] Muhammad Irfan Majeed, *[a] Haq Nawaz, *[a] Abeer Ahmed Alghamdi,*[b] Muhammad Adnan Iqbal,[a] Muhammad Shahid,[c] Urwa Shahid,[a] Rabiea Umer,[a] Muhammad Tjammal Rehman,[c] Umer Farooq,[a] Ahmad Hassan[a] and Muhammad Imran [d]

Escherichia coli biofilms are a major cause of gastrointestinal tract diseases, such as esophageal, stomach and intestinal diseases. Nowadays, these are the most commonly occurring diseases caused by consuming contaminated food. In this study, we evaluated the efficacy of probiotics in controlling multidrug-resistant *E. coli* and reducing its ability to form biofilms. Our results substantiate the effective use of probiotics as antimicrobial alternatives and to eradicate biofilms formed by multidrug-resistant *E. coli*. In this research, surface enhanced Raman spectroscopy (SERS) was utilized to identify and evaluate *Escherichia coli* biofilms and their response to the varying concentrations of the organometallic compound bis(1,3-dihexylimidazole-2-yl) silver(I) hexafluorophosphate (V). Given the escalating challenge of antibiotic resistance in bacteria that form biofilms, understanding the impact of potential antibiotic agents is crucial for the healthcare sector. The combination of SERS with principal component analysis (PCA) and partial least squares discriminant analysis (PLS-DA) enabled the detection and characterization of the biofilm, providing insights into the biochemical changes induced by the antibiotic candidate. The identified SERS spectral features served as indicators for elucidating the mode of action of the potential drug on the biofilm. Through PCA and PLS-DA, metabolic variations allowing the differentiation and classification of unexposed biofilms and biofilms exposed to different concentrations of the synthesized antibiotic were successfully identified, with 95% specificity, 96% sensitivity, and a 0.75 area under the curve (AUC). This research underscores the efficiency of surface enhanced Raman spectroscopy in differentiating the impact of potential antibiotic agents on *E. coli* biofilms.

Received 19th December 2023
Accepted 23rd January 2024

DOI: 10.1039/d3ra08667d

rsc.li/rsc-advances

1. Introduction

E. coli bacterial strains are primarily responsible for morbidity and mortality due to infections associated with biomedical apparatuses, including urethral and intravascular catheters, prosthetic joints, shunts, and grafts.[1] *E. coli* is a communal organism that can form biofilms, which are a collection of microorganisms that coexist as a community and are frequently found adhered to solid surfaces in damp environments. Extracellular polymeric substances (EPSs), a class of protective compounds secreted by microbes in biofilms, help microbes to survive. *Escherichia coli* biofilms have been found to be the primary pathogenic agent in many intestinal infections.[2]

After the development of a biofilm, bacteria produce a range of biopolymers that help in cell-to-cell and cell-to-surface attachment. These extracellular polymeric substances (EPSs), which are primarily made up of proteins, lipids, polysaccharides, and nucleic acids, help in the mechanical stability and adhesion of biofilms to surfaces. Additionally, they serve as scaffolds for three-dimensional biofilm structures that unite and immobilize the bacterial community.[3] In medical settings, biofilms release toxic substances and can even impede catheters

[a]*Department of Chemistry, University of Agriculture Faisalabad, Faisalabad 38000, Pakistan. E-mail: irfan.majeed@uaf.edu.pk; haqchemist@yahoo.com*

[b]*Department of Physics, College of Science, Princess Nourah bint Abdulrahman University, P.O. Box 84428, Riyadh 11671, Saudi Arabia. E-mail: abaalghamdi@pnu.edu.sa*

[c]*Department of Biochemistry, University of Agriculture Faisalabad, Faisalabad 38000, Pakistan. E-mail: abaalghamdi@pnu.edu.sa*

[d]*Department of Chemistry, Faculty of Science, King Khalid University, P.O. Box 9004, Abha 61413, Saudi Arabia*

† Electronic supplementary information (ESI) available. See DOI: https://doi.org/10.1039/d4ta00235k

‡ First two authors have equal contribution.

due to persistent infections, accounting for 80% or more of all bacterial infections.[4] *E. coli* is a principal factor responsible for sepsis in neonates and individuals with a weak immune system. Particularly, the pathogenicity of *E. coli* depends on its capacity to build biofilms rather than the toxins it produces.[5] M13 stands out as a promising naturally occurring biorecognition element candidate for targeting *E. coli*.[6,7] Conventional biological recognition elements, such as aptamers, antibodies, and peptides, exhibit high specificity towards targeted bacteria. However, they are vulnerable to damage under conditions like elevated temperature, high salt concentration, acidic pH, chaotropic agents, and prolonged storage.[7,8]

Quorum sensing (QS), a chemical signaling mechanism, is used by the densely packed bacterial cells in biofilms to interact with one another. When the required cell density is reached, bacteria release autoinducer chemicals into the extracellular matrix to upregulate the development and maturation of biofilms.[9] Autoinducer molecules play an important role in facilitating the secretion of virulence factors by the bacterial cells within the biofilm, thereby modulating the host immune system. The biofilm presents a challenging barrier as it impedes the penetration of conventional antibiotics and consequently reduces their efficacy against the bacterial cells.[10,11] Therefore, it is urgent to look into alternative therapeutic agents to treat diseases that are caused, in particular, by the development of *E. coli* biofilms.

Characterization of bacteria and their biofilms is generally performed by using nuclear magnetic resonance (NMR) spectroscopy,[12] infrared (FTIR) spectroscopy,[13] mass spectrometry[14] and X-ray crystallography[15] techniques. Although these techniques can provide information about the biochemistry of biofilms, they have some limitations. Because of very high energy, X-ray crystallography can destroy materials if they are not in powder form. The NMR and FTIR techniques need rigorous sample preparation and are not appropriate for samples containing water molecules. For the characterization and identification of biofilms and bacteria, Christensen's method,[16] polymerase chain reaction[17] and Congo red staining[18] methods can be utilized, but they are time-consuming and need many consumables. The development of novel, fast identification techniques that require minimal or no sample preparation to differentiate between bacteria and biofilms is urgently needed.[19] In this work, we evaluated the efficacy of probiotics in controlling multidrug-resistant *E. coli* and reducing their ability to form biofilms. Our results validate the effective use of probiotics as antimicrobial alternatives and to eradicate biofilms formed by multidrug-resistant *E. coli*.[20]

Raman spectroscopy is considered a quick method for the identification and characterization of bacteria,[21] but it faces the problem of weak Raman signals.[22] However, this can be resolved by using surface-enhanced Raman spectroscopy, which delivers specific biochemical information and is regarded to have substantial potential to characterize and identify bacteria.[23,24] Surface-enhanced Raman spectroscopy (SERS) was introduced by Fleischmann *et al.* in 1974 as a robust vibrational spectroscopic method.[25] This innovative technique enables exceptionally sensitive identification of individual molecules regardless of the presence of water molecules.[26–28] Its application has extended significantly to optics and interface science. SERS expands the capabilities of Raman spectroscopy beyond its limitations related to low concentrations and sensitivity. Its practical applications have diversified, encompassing environmental monitoring,[29,30] food safety analysis,[31,32] national security surveillance,[33] and biomedical research.[34–38] SERS has also been employed to investigate the interaction mechanism between ASOs and SARS-CoV-2 RNA in combination with machine learning techniques.[39] SERS employs nanoparticles as the substrate to boost the Raman signal and has different applications in bacterial analysis, including the identification of drug-sensitive/drug-resistant bacterial strains and food-processing bacteria.[40–42] A sensitive and convenient SERS platform that provides tunable lipid monolayer/bilayer environments for the investigation of protein secondary structures during protein–membrane interactions under low physiological concentrations has been described previously.[43]

Silver nanoparticles (Ag NPs) have been used as the SERS substrate to enhance the Raman signal in studies on diverse microorganisms.[44] As there are more active sites in silver nanoparticles than gold nanoparticles, the surface plasmon resonance is amplified and can lead to a stronger SERS enhancement.[45]

The biofilms of different bacteria, including *E. coli*, *C. albicans*, *P. aeruginosa*, and *S. epidermidis*, have been characterized by surface-enhanced Raman spectroscopy.[46,47] Surface-enhanced Raman spectroscopy (SERS) serves as a promising analytical method for rapid and precise disease detection owing to its appealing features.[48] Given the difficulty in developing a highly sensitive and rapid method for bacterial identification and drug-resistance detection, the use of surface-enhanced Raman scattering (SERS) has garnered growing interest as a potent bioanalytical tool for bacterial detection.[49] In this study, surface-enhanced Raman spectroscopy is used in conjunction with chemometric techniques, specifically Principal Component Analysis (PCA) and Partial Least Squares Discriminant Analysis (PLS-DA), to identify and characterize the biochemical changes caused by the interaction of a potential antibacterial agent, namely bis(1,3-dihexylimidazole-2-yl) silver(I) hexafluorophosphate (V), with the biofilm of *E. coli* bacteria. Notably, our work proposes a novel method to identify novel antibacterial agents that are effective against biofilm-forming bacterial strains, for the first time.

2 Materials and methods

The chemicals required for synthetic work, including benzimidazole, benzyl bromide, and potassium hydroxide, were obtained from Alfa Aesar. Silver(I) oxide and KPF_6 were purchased from Alfa Aesar. The solvents used, namely methanol, ethanol, dimethyl sulfoxide (DMSO), *n*-hexane, 1,4 dioxane, chloroform, and carbon tetrachloride, were purchased from Sigma Aldrich.

2.1. Synthesis of bis(1,3-dihexylimidazole-2-yl) silver(I) hexafluorophosphate (V)

A previously reported method was used, with minor modification, to prepare an imidazole-based compound.[50] Methanol (50–

60 mL) was used to dissolve 1 g of imidazolium salt (3.469 mM) and 1 g of silver oxide (4.314 mM). The mixture was stirred for 48 hours, while the round-bottom flask was covered with aluminum foil to prevent light exposure. To get a clear solution, the mixture was filtered through Celite (545) when the reaction was completed. KPF_6 (1 g, 5.432 mM) was gradually added to the above-mentioned complex solution prepared in methanol (30–40 mL) in a different round-bottom flask. The solution was stirred for 1 h, and the obtained precipitates were filtered and washed with distilled water and methanol. The complex was dried at RT for several days and ground to a fine powder. Yields 82%, M. P. 252 °C, ^{1}H NMR (600 MHz DMSO-d_6, δ ppm), 0.85 (t, 12H, 4 × CH_3), 1.28 (m, 16H, 4 × 2 (CH_2)), 1.32 (m, 8H, 4 × CH_2), 1.38 (m, 8H, 4 × CH_2), 2.55 (t, 8H, 4 × CH_2–N), 4.28 (m, 4H, 4×Aliph-H). ^{13}C NMR (150 MHz, DMSO-d_6, δ ppm), 13.3 (CH_3), 18.8, 27.5, 29.3, 33.2 (CH_2), 53.4 (CH_2–N), 122.3 (C-Aliph), 173.5 (C–Ag).

The synthesis, ^{1}H NMR and ^{13}C NMR results of bis(1,3-dihexylimidazole-2-yl) silver(I) hexafluorophosphate (V) compound are discussed in Scheme 1, Fig. 1 and 2, respectively, in Section 2.1 of the ESI.†

2.2. Formation of biofilms

The bacterial isolate (*Escherichia coli*) is obtained from the institutional stock cultures. 2.1 g Muller Hinton Broth powder was added to a flask and made up to 100 mL using distilled water to prepare the growth medium. The flask was sterilized in an autoclave at 121 °C, 15P and for 15 min and then placed at room temperature for cooling. Each well of the ELISA plate was filled with 1 mL of broth and incubated overnight in a rotatory shaker at 37 °C for 24 hours. After this, the bacterial biofilms were exposed to different concentrations of the lab-synthesized potential antibacterial agent (organometallic compound) bis(1,3-dihexylimidazole-2-yl) silver(I) hexafluorophosphate (V) to check its activity against the biofilm.

2.3. Synthesis and characterization of silver nanoparticles (Ag NPs)

Silver nanoparticles were prepared by the chemical reduction method and used as the SERS substrate. In this method, trisodium citrate $Na_3C_6H_5O_7$ (a reducing agent) and silver nitrate $AgNO_3$ (precursor) were used. In 100 mL of distilled water, 0.017 g of $AgNO_3$ was heated at 100 °C, followed by the addition of 0.025 g of $Na_3C_6H_5O_7$. The mixture was heated on a hot plate using a magnetic stirrer for approximately an hour until gray-colored silver nanoparticles in the size range of 65 × 45 nm were formed, as characterized and reported earlier.[51] The SEM analysis was performed to characterize the Ag NPs as shown in Fig. S1† and discussed in Section 2.2 in ESI.†

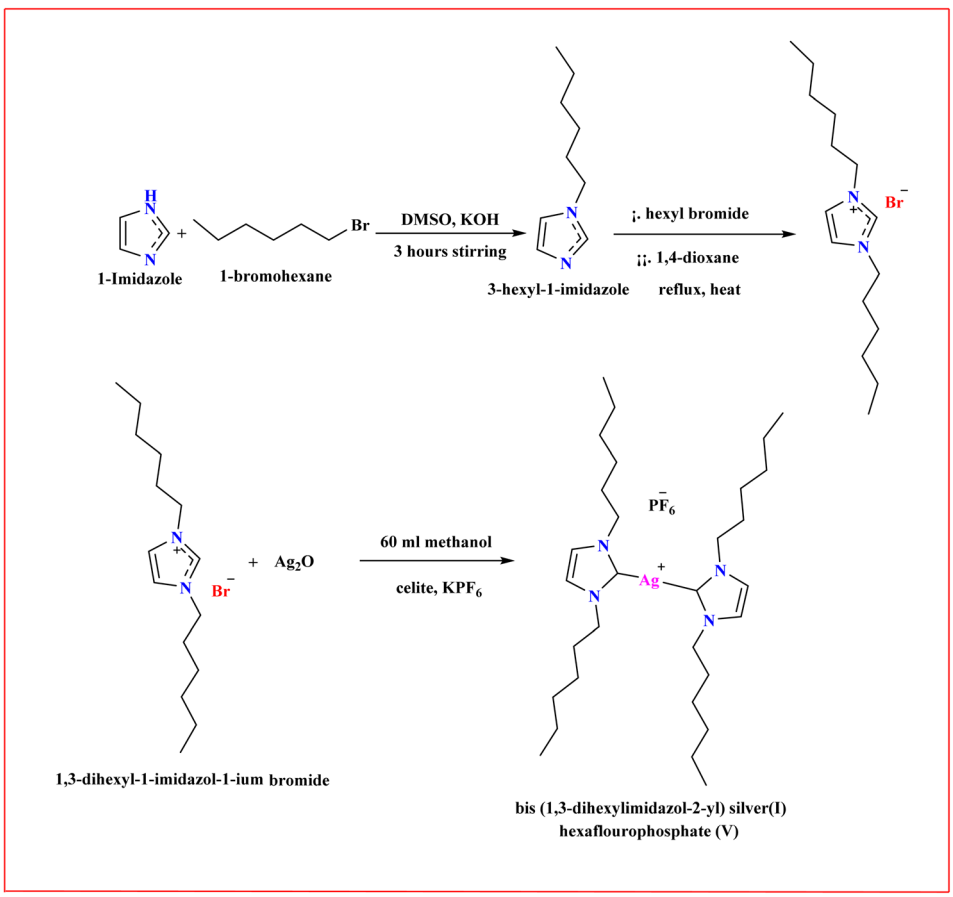

Scheme 1 Synthesis of bis(1,3-dihexylimidazole-2-yl) silver(I) hexafluorophosphate (V).

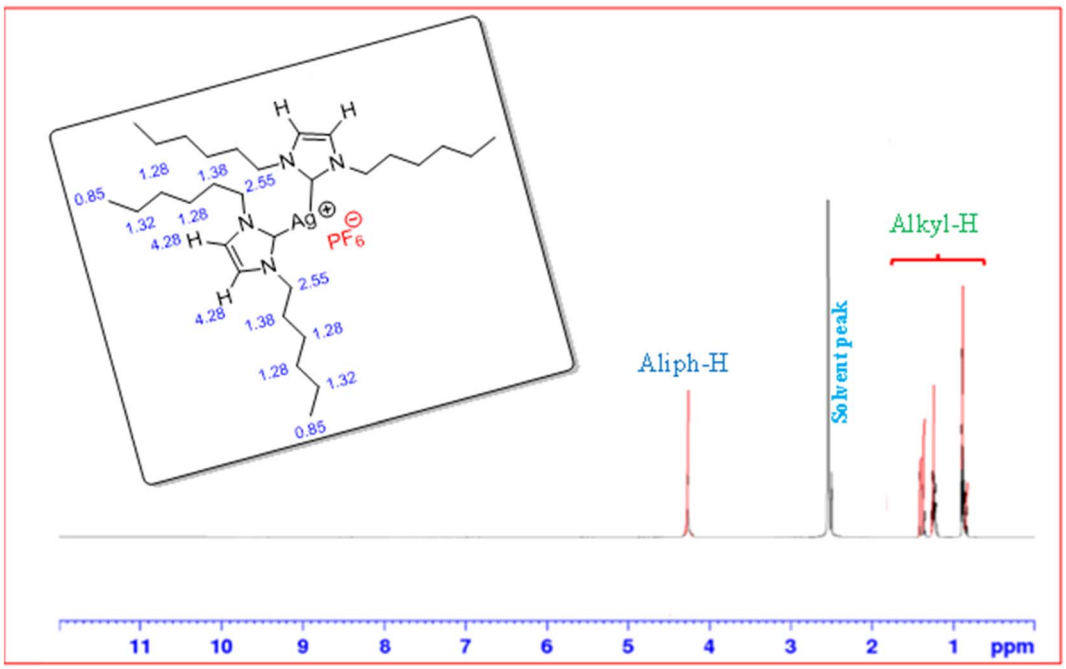

Fig. 1 ^{1}H NMR spectrum of bis(1,3-dihexylimidazole-2-yl) silver(I) hexafluorophosphate (V).

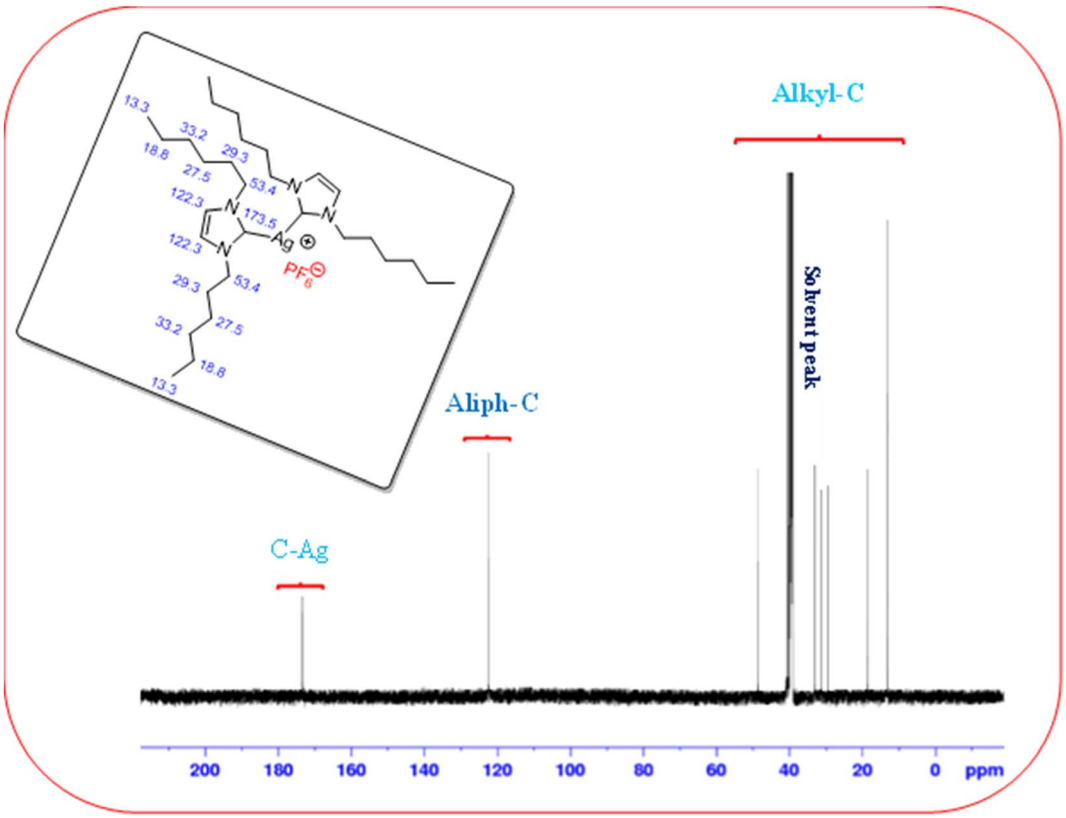

Fig. 2 ^{13}C NMR spectrum of bis(1,3-dihexylimidazole-2-yl) silver(I) hexafluorophosphate (V).

2.4. SERS spectral acquisition

For acquiring the SERS spectra, each biofilm sample was suspended in an equal volume of the saline solution. 50 μL of each sample was mixed with 50 μL of Ag NPs in an Eppendorf and incubated for 30 minutes. From this mixture, 50 μL was taken on an aluminum slide for SERS spectral studies. SERS spectral acquisition was carried out using a Raman microscope spectrometer (ATR8300BS), Optosky China, with

a 785 nm laser that delivers a laser light of 150 mW power on the sample through a 20× objective lens. An integration time of 10 seconds was applied to capture 15 Raman spectra in the 400–1600 cm^{-1} wavenumber range for all bacterial biofilm samples.

2.5. Pre-processing of SERS data

SERS signals generally include undesirable components, such as background/substrate contribution, baseline and noise, which can obstruct the discernment of specific information about the sample under study. To extract desirable information from the SERS spectral data, pre-processing was carried out by using MATLAB software version 7.8 (R2009a).[52]

Data pre-processing involved four steps, including substrate removal, vector normalization, smoothing of data and baseline correction. After baseline correction of spectral data using polynomial and rubber band correction techniques, the Savitzky–Golay algorithm was utilized to smoothen the SERS signals.

2.6. SERS data analysis

Various chemometric techniques, including PCA and PLS-DA, were employed to analyze the processed Surface-Enhanced Raman Scattering (SERS) data, particularly in the context of multivariate spectral datasets. These methods helped in the identification of distinct SERS spectral characteristics related to the biochemical changes in *E. coli* biofilms induced by the antibacterial agent. To explore differentiation and variability across datasets, PCA scatter plots and PCA loadings were performed with the SERS spectral data from *E. coli* biofilms. The dimensionality decreased with PCA, but variability remained unaltered. The correlated variables were transformed into uncorrelated variables by this qualitative analysis method, in which the primary principal component (PC-1) explains the majority of variance in the datasets, while the remaining variability is explained by PC-2.

A flexible and supervised modelling technique (PLS-DA) was used to calibrate and validate the multivariate discriminant models obtained from the SERS spectral data sets to determine the impact of the antibacterial drug on *E. coli* biofilms. This model constructs a classification using spectral data comparing *x*- and *y*-variables. After combining all the spectral data into a matrix, the randomization command was utilized to eliminate bias. Then, data were divided into calibration sets and validation sets, each comprising 80% and 20% of the total data. Cross-validation was performed using Monte Carlo cross-validation.

The receiver operating characteristic (ROC) curve is frequently used to assess the effectiveness of binary classification systems. There are four possible results for binary classification, including true positives, false positives, true negatives and false negatives. After determining the true positive rate (sensitivity) and false positive rate (specificity), the ROC curve was plotted. Sensitivity is determined as the ratio of true positive samples to the combined forms of samples (true positive and false negative) on the *y*-axis. It was determined using the below formula:

$$\mathrm{TPR} = \text{sensitivity} = \frac{\text{true positive}}{\text{true positive} + \text{false negative}}$$

Specificity is determined as the ratio of false positive samples to the combined forms of samples (false positive and true negative) on the *x*-axis. It was determined as:

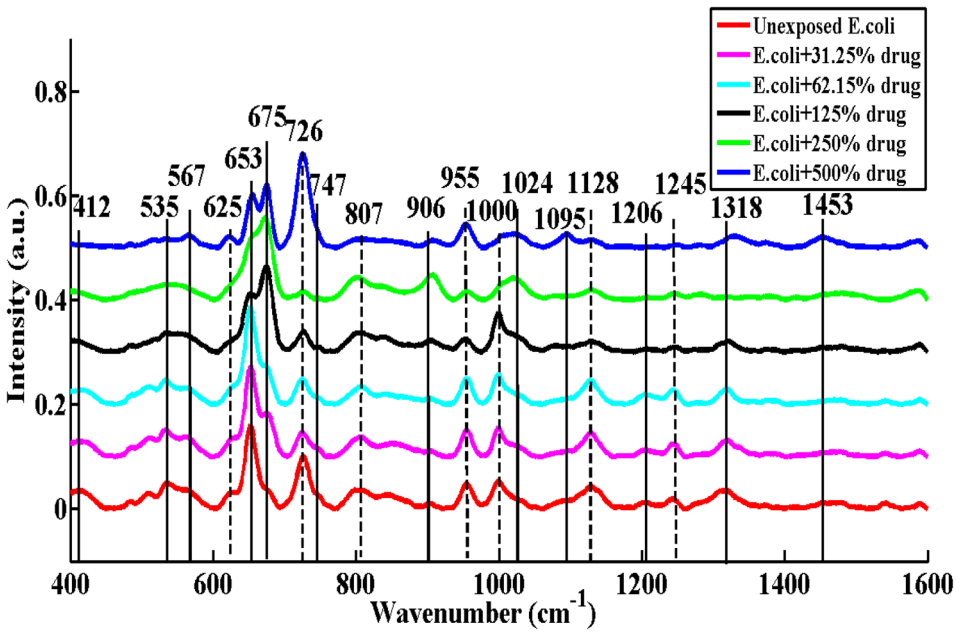

Fig. 3 Mean SERS spectra of the unexposed *Escherichia coli* biofilm and those exposed to various concentrations of the lab-synthesized antibacterial agent bis(1,3-dihexylimidazole-2-yl) silver(I) hexafluorophosphate (V).

$$\text{FPR} = \text{specificity} = \frac{\text{false positive}}{\text{false positive} + \text{true negative}}$$

Or

$$\text{FPR} = \text{specificity} = 1 - \text{sensitivity}$$

3 Results and discussion

3.1. Mean SERS spectra

According to the diverse biomolecular components, the mean SERS plot in Fig. 3 shows several SERS spectral features that distinguish the impact of the antibacterial agent on the *E. coli* biofilm. The majority of the biochemical components are linked

Table 1 Assignment of SERS peaks indicating the effect of the antibacterial agent bis(1,3-dihexylimidazole-2-yl) silver(I) hexafluorophosphate (V) on *E. coli* biofilms

SERS peaks (cm^{-1})	Peak assignments	Components	References
412	Carbohydrate	Carbohydrate	53
535	Guanine	DNA/RNA	54
567	Adenine	DNA/RNA	54
625	Hypoxanthine	DNA/RNA	54
653	Xanthine	DNA/RNA	54
675	C–S stretching and C–C twisting of proteins (tyrosine)	Protein	55
726	Ring breathing	DNA/RNA	56
747	Thymine	DNA/RNA	57
807	*n*(CC) ring breathing (DNA)	DNA/RNA	58
906	Vibration of the epoxide ring in GMA	Lipids	59
955	Xanthine	DNA/RNA	54
1000	Protein	Protein	47
1024	Hypoxanthine	DNA/RNA	54
1095	DNA: O–P–O^-	DNA/RNA	60
1128	Guanine	DNA/RNA	54
1206	Protein	Protein	61
1245	Adenine ring-breathing mode	DNA/RNA	62
1318	Guanine breathing ring, DNA	DNA/RNA	63
1453	Amide band (C=O vibration)	Proteins	64

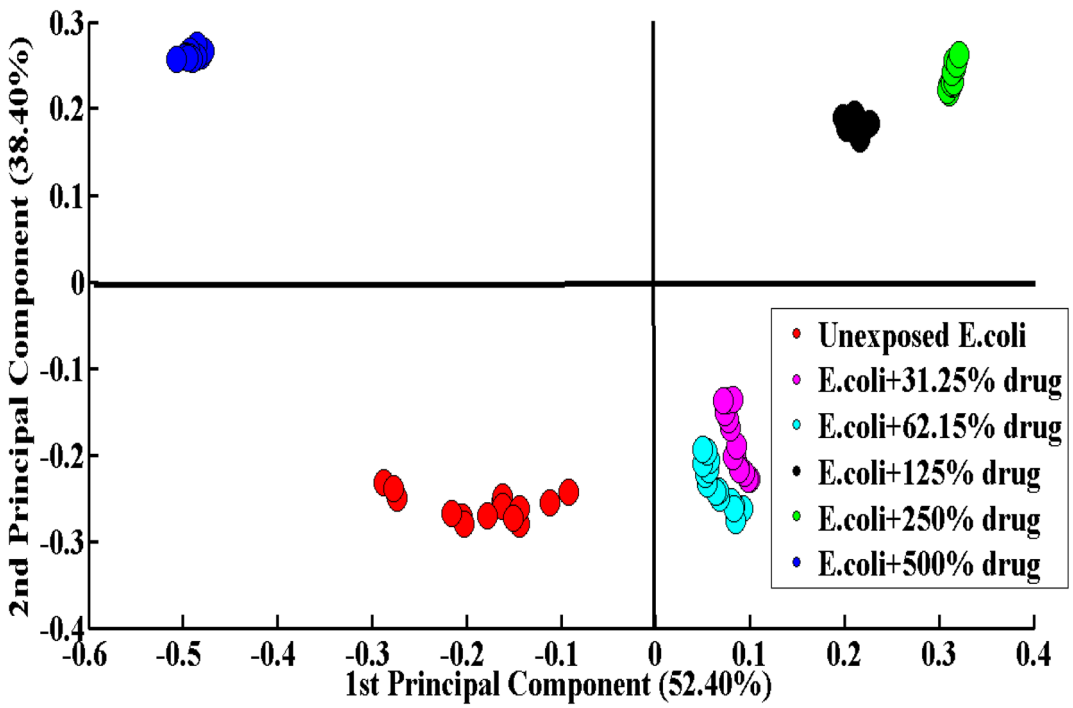

Fig. 4 PCA scatter plot of the SERS spectra of *Escherichia coli* biofilms demonstrating the effect of different concentrations of the antibacterial drug bis(1,3-dihexylimidazole-2-yl) silver(I) hexafluorophosphate (V).

to amino acids, carbohydrates, lipids, proteins and DNA/RNA. The solid lines indicate the discriminating SERS bands, while the dotted lines indicate SERS bands with intensity-based differences. In the mean plot, six samples are represented by different colors; red represents the SERS spectrum of the unexposed *E. coli* biofilm, and the remaining five spectra are those of the bacterial biofilms exposed to different concentrations of the antibacterial agent. Purple represents 31.25%, cyan represents 62.15%, black represents 125%, green represents 250% and blue represents 500% antibacterial concentration.

In Fig. 3, the SERS differentiating bands include those found at 412 cm^{-1} (carbohydrates), 535 cm^{-1} (guanine), 567 cm^{-1} (adenine), 653 cm^{-1} (xanthine), 675 cm^{-1} (C–S stretching and C–C twisting of proteins (tyrosine)), 747 cm^{-1} (thymine), 906 cm^{-1} (vibration of the epoxide ring in GMA), 1024 cm^{-1} (hypoxanthine), 1095 cm^{-1} (DNA: O–P–O^-), 1206 cm^{-1} (proteins), 1318 cm^{-1} (guanine breathing ring, DNA) and 1453 cm^{-1} (amide band (C═O vibration)) (Table 1).

The SERS features labelled by dotted lines show differences based on intensity due to the effect of the antibacterial agent. These SERS features include 625 cm^{-1} (hypoxanthine), 726 cm^{-1} (ring breathing), 807 cm^{-1} (*n*(CC) ring breathing (DNA)), 955 cm^{-1} (xanthine), 1000 cm^{-1} (proteins), 1128 cm^{-1} (guanine) and 1245 cm^{-1} (adenine ring-breathing mode).

It is evident that the intensity of DNA-related peaks had changed. The intensity of the SERS bands at 567, 726, 1024 and 1095 cm^{-1} increased as the concentration of the lab-synthesized antibacterial drug increased. This also indicates that adenine and adenine-containing molecules and the ring breathing mode of purine increased as the concentration of the lab-synthesized drug increased. The intensity of the SERS bands at 535, 747, 807, 1128 and 1245 cm^{-1} decreased as the concentration of the lab-synthesized antibacterial drug increased, representing the disintegration of DNA.

Several peaks, such as 675, 1000 and 1206 cm^{-1}, could be assigned to proteins and indicated solid and intensity-based differences. The intensity of the SERS band at 675 cm^{-1} increased as the concentration of the lab-synthesized antibacterial drug increased. The intensity of the SERS bands at 1000 and 1206 cm^{-1} decreased as the concentration of the lab-

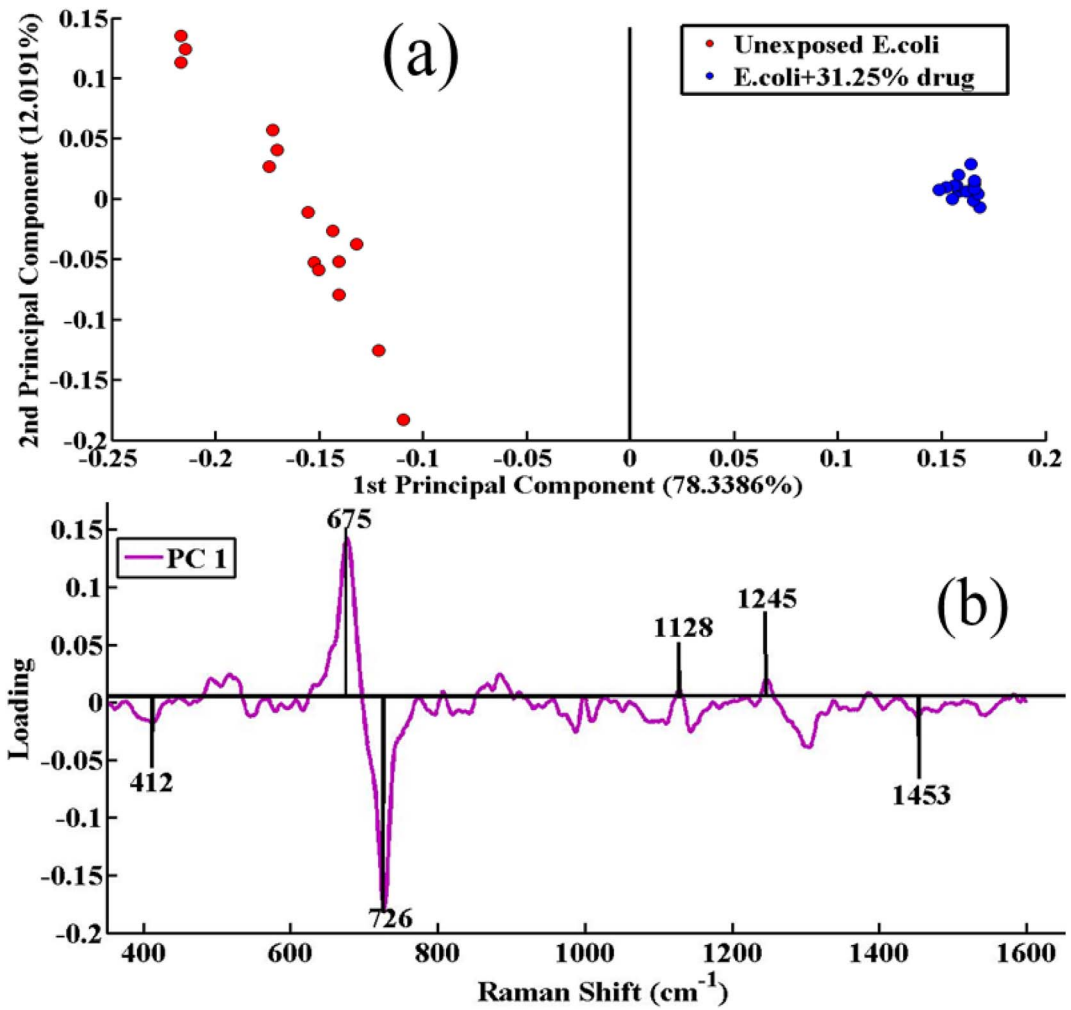

Fig. 5 (a) Pairwise PCA and (b) scatter plot loadings of the unexposed *Escherichia coli* biofilm and the biofilm exposed to the lowest concentration (31.25%) of the antibacterial drug bis(1,3-dihexylimidazole-2-yl) silver(I) hexafluorophosphate (V).

synthesized antibacterial drug increased, indicating the denaturation of proteins, which leads to cell death. The SERS peak related to carbohydrates detected at 412 cm^{-1} decreased in intensity as the concentration of the lab-synthesized antibacterial drug increased.

The peaks of the SERS associated with lipids found at 906 cm^{-1} (vibration of the epoxide ring in GMA) and 1453 cm^{-1} (amide band (C═O vibration)) increased in intensity as the concentration of the lab-synthesized antibacterial drug increased. These peaks are directly associated with the enhanced rate of saturation of unsaturated fatty acids in bacterial cells and amides after the application of the antibacterial drug. These lipids and proteins are considered useful in bacterial quorum sensing, a mechanism of communication among bacteria within the biofilm.[65]

3.2. Principal component analysis (PCA)

Principle component analysis was employed to differentiate the spectral features of the bacterial biofilm samples exposed to different antibiotic concentrations from those of the unexposed biofilm. Fig. 4 displays the PCA scatter plot of all the SERS spectra. The purple, cyan, black and green dot clusters represent the spectral data sets of the different drug concentrations, namely 31.25, 62.15, 125 and 250%, respectively, and were present on the positive side of PC-1. The red and blue dots represent the spectral features of the unexposed *E. coli* biofilm and at 500% drug concentration, respectively; they were grouped together on the negative side of PC-1 in the scatter plot.

Fig. 5(a) represents the pairwise scatter plot analysis of the SERS spectra of the unexposed *E. coli* biofilm (red) and that exposed to 31.25% antibacterial drug (blue). It demonstrates a significant difference between the two. The red cluster seen on the negative side of PC-1 is related to the SERS spectra of the unexposed *E. coli* biofilm, while the blue cluster present on the positive side of PC-1 is related to the SERS spectral features of the biofilm exposed to the lab-synthesized drug (31.25%). The variability through PC-1 was 78.33% while the variability explained by PC-2 is 12.01%. Fig. 5(b) represents the pairwise

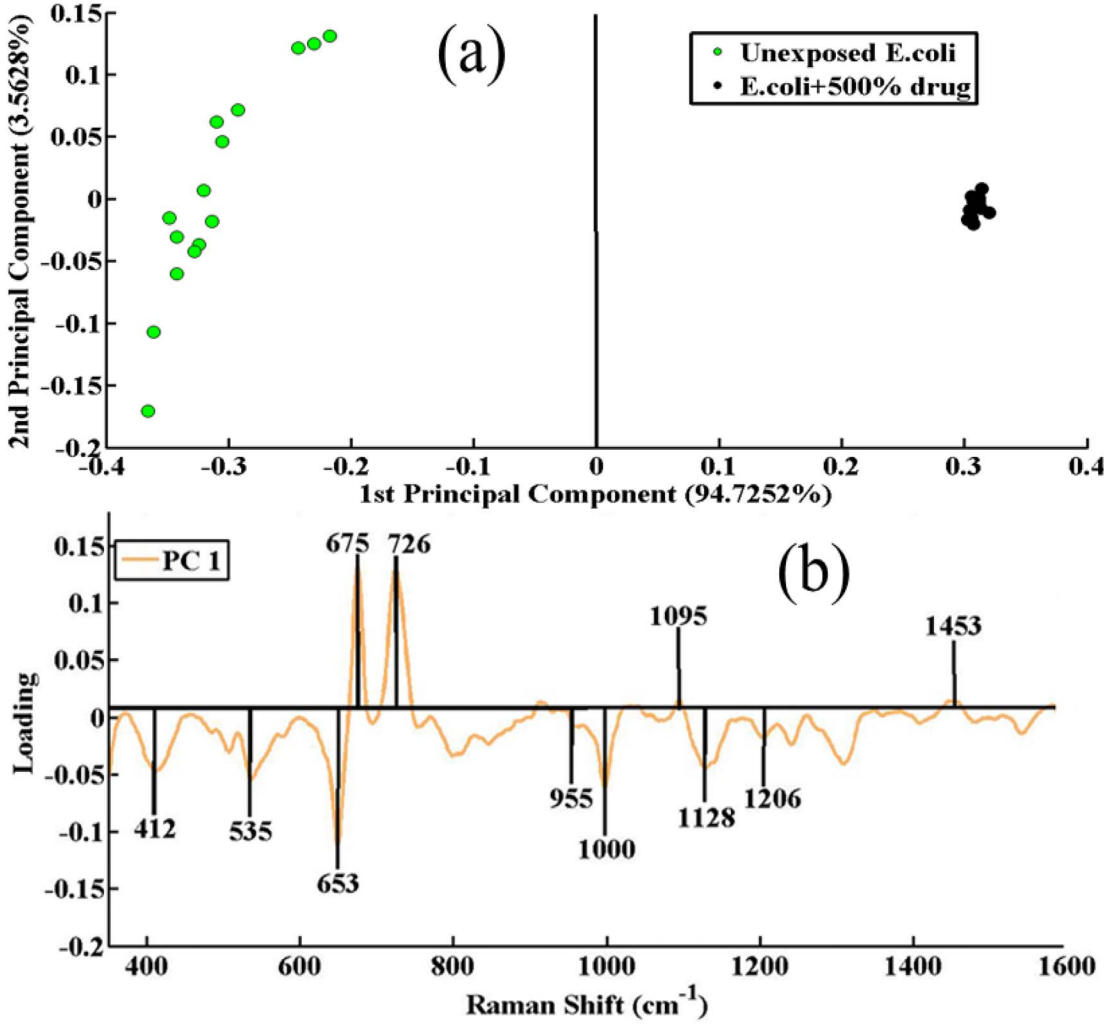

Fig. 6 Principal component analysis (PCA) pairwise visualization: (a) scatter plot and (b) loadings comparing the unexposed *Escherichia coli* biofilm with the biofilm exposed to the highest concentration (500) of the antibacterial drug bis(1,3-dihexylimidazole-2-yl) silver(I) hexafluorophosphate (V).

PCA loadings of the SERS spectral data sets of the unexposed *E. coli* biofilm and that exposed to the lowest concentration of the lab-synthesized drug. The comparative SERS analysis shows clear differences between the exposed and unexposed bacterial biofilms. The negative loadings, including 412 cm^{-1} (carbohydrates), 726 cm^{-1} (ring breathing) and 1453 cm^{-1} (amide band (C═O vibration)), are associated with the SE unexposed *E. coli* biofilm. The positive loadings, including 675 cm^{-1} (C–S stretching and C–C twisting of proteins (tyrosine)), 1128 cm^{-1} (guanine) and 1245 cm^{-1} (adenine ring-breathing mode), are related to the biofilm exposed to the lowest concentration of the lab-synthesized antibacterial drug (31.25%).

Fig. 6(a) represents the comparative scatter plot of unexposed *E. coli* (green) and the biofilm exposed to 500% antibacterial drug (black). A significant difference can be seen between these groups. The green cluster present on the negative side of PC-1 is related to the SERS spectra of the unexposed *E. coli* biofilm, while the black cluster present on the positive side of PC-1 is related to the SERS spectra of the biofilm exposed to 500% lab-synthesized drug. In this case, 94.72% of the variability was explained by PC-1, while 3.56% of the variability was explained by PC-2. Fig. 6(b) represents the pairwise PCA loadings of the SERS spectral data sets of the unexposed *E. coli* biofilm and the biofilm exposed to the highest concentration of the lab-synthesized drug. The SERS analysis shows clear differences between the exposed and unexposed bacterial biofilms.

The negative loadings, including 412 cm^{-1} (carbohydrates), 535 cm^{-1} (guanine), 653 cm^{-1} (xanthine), 955 cm^{-1} (xanthine), 1000 cm^{-1} (proteins), 1128 cm^{-1} (guanine) and 1206 cm^{-1} (proteins) are associated with the unexposed *E. coli* biofilm. The positive loadings, including 675 cm^{-1} (C–S stretching and C–C twisting of proteins (tyrosine)), 726 cm^{-1} (ring breathing), 1095 cm^{-1} (DNA: O–P–O^{-}) and 1453 cm^{-1} (amide band (C═O vibration)), correlate with the sample exposed to the highest concentration of the lab-synthesized antibacterial drug *i.e.*, 500%.

3.3. Partial least squares discriminant analysis (PLS-DA)

The PLS-DA model is helpful for differentiation, quantitative classification and calculating the sensitivity and specificity of the SERS technique for a specific purpose. In this study, this model was used for the classification of the spectral attributes of the unexposed *E. coli* biofilm and those exposed to various doses of the antibacterial agent. The chosen number of latent variables for this purpose was 5, and the calibration and validation data accounted for 80% and 20%, respectively.

Fig. 7 illustrates the score plot of the PLS-DA model obtained for the six classes of SERS data sets belonging to the unexposed *E. coli* biofilm and biofilms exposed to different doses of the lab-synthesized antibacterial compound. The SERS spectral features of the unexposed *E. coli*, and *E. coli* biofilms exposed to different doses of the lab-synthesized compound (represented by different colors) are seen on the positive side of the score plot.

The area under the receiver operating characteristics (ROC) curve was 0.75, as seen in Fig. 8, based on the analysis of the SERS spectral features of the biofilms through PLS-DA. The range of this model is 0 to 1; if the value is close to 1, the model is more accurate, as 1 represents the highest level of validity and accuracy. The suggested model displays outstanding performance in identifying the *E. coli* biofilm and the impact of various doses of the synthesized compound on the *E. coli* biofilms using SERS data sets.

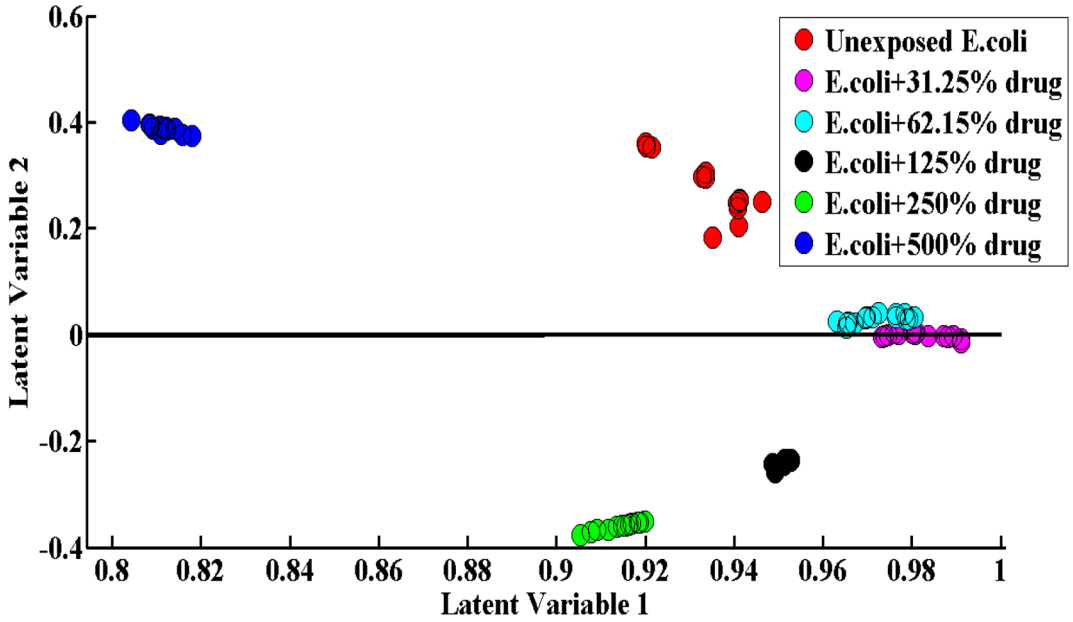

Fig. 7 Score plot of the PLS-DA model of the SERS data sets of the unexposed *E. coli* biofilm and biofilms exposed to various doses of the lab-synthesized antibacterial drug bis(1,3-dihexylimidazole-2-yl) silver(I) hexafluorophosphate (V).

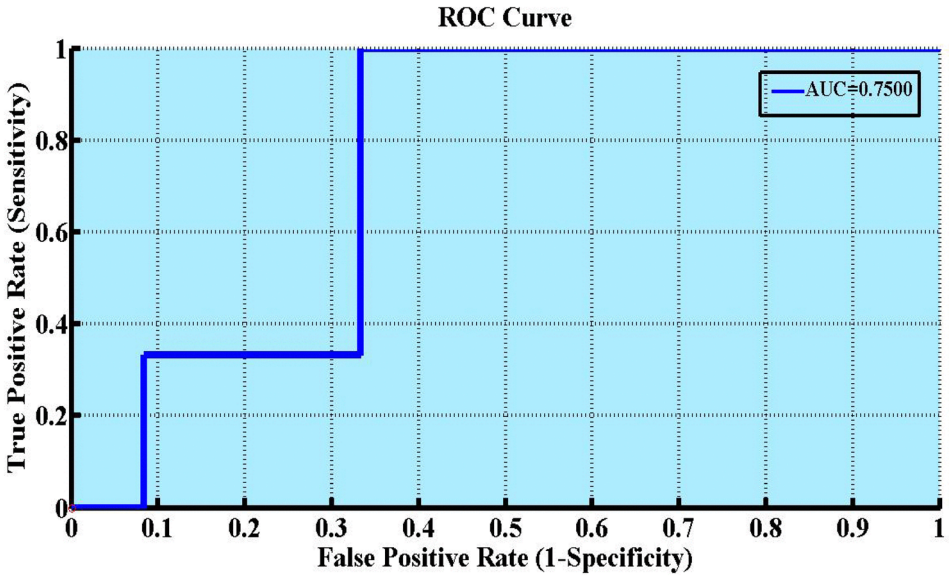

Fig. 8 Receiver operating characteristic (ROC) curve of the partial least squares discriminant analysis (PLS-DA) model applied to the surface-enhanced Raman spectroscopy (SERS) spectral datasets pertaining to *Escherichia coli* biofilms. The curve depicts the impact of different concentrations of the compound bis(1,3-dihexylimidazole-2-yl) silver(I) hexafluorophosphate (V) on the biofilm.

4 Conclusion

In this work, surface-enhanced Raman spectroscopy (SERS) emerges as a valuable technique for categorizing SERS spectral datasets associated with both unexposed and drug-exposed *Escherichia coli* biofilms at varying concentrations of a laboratory-synthesized compound. The SERS spectra obtained from the different bacterial biofilm samples were used to identify the distinctive SERS spectral features related to the different biochemical changes that take place in the bacterial biofilm. The SERS spectral data sets of the *E. coli* biofilm and the impact of different concentrations of the lab-synthesized compound bis(1,3-dihexylimidazole-2-yl) silver(I) hexafluorophosphate (V) on biofilm were categorized using PCA and PLS-DA models. These SERS peaks linked to key biomolecules like lipids, carbohydrates, nucleic acids, and proteins were identified. The distinguishing SERS bands (solid lines in the mean plot) included 412 cm^{-1} (carbohydrates), 535 cm^{-1} (guanine), 567 cm^{-1} (adenine), 653 cm^{-1} (xanthine), 675 cm^{-1} (C–S stretching and C–C twisting of proteins (tyrosine)), 747 cm^{-1} (thymine), 906 cm^{-1} (vibration of the epoxide ring in GMA), 1024 cm^{-1} (hypoxanthine), 1095 cm^{-1} (DNA: O–P–O^-), 1206 cm^{-1} (proteins), 1318 cm^{-1} (guanine breathing ring, DNA) and 1453 cm^{-1} (amide band (C=O vibration)). The SERS features labelled by the dotted lines show intensity-based differences due to the effect of the antibacterial agent. These SERS features included 625 cm^{-1} (hypoxanthine), 726 cm^{-1} (ring breathing), 807 cm^{-1} (*n*(CC) ring breathing (DNA)), 955 cm^{-1} (xanthine), 1000 cm^{-1} (proteins), 1128 cm^{-1} (guanine) and 1245 cm^{-1} (adenine ring-breathing mode). This quantitative approach enables precise discrimination of different concentrations of the antibacterial agent against *E. coli* biofilms based on SERS spectral data. Given the sensitivity of 96%, specificity of 95%, area under the curve (AUC) of 0.75, precision of 97%, and accuracy of 98%, Partial Least Squares Discriminant Analysis (PLS-DA) proves to be a valuable method for discriminating and identifying diverse spectral data associated with *E. coli* biofilms, as well as for assessing the influence of varying antibiotic doses.

Conflicts of interest

The authors have no known competing financial interests or personal relationships that could have appeared to influence the work reported in this paper.

Acknowledgements

The authors express their gratitude to Princess Nourah bint Abdulrahman University Researchers Supporting Project number (PNURSP2024R451), Princess Nourah bint Abdulrahman University, Riyadh, Saudi Arabia. M. Imran expresses his appreciation to the Deanship of Scientific Research at King Khalid University, Saudi Arabia, for funding this work through the research group program under grant number RGP-2/570/44.

References

1 A. Reisner, M. Maierl, M. Jörger, R. Krause, D. Berger, A. Haid, D. Tesic and E. L. Zechner, *J. Bacteriol.*, 2014, **196**, 931–939.
2 N. Allocati, M. Masulli, M. F. Alexeyev and C. Di Ilio, *Int. J. Environ. Res. Public Health*, 2013, **10**, 6235–6254.
3 T. Das, S. Sehar, L. Koop, Y. K. Wong, S. Ahmed, K. S. Siddiqui and M. Manefield, *PLoS One*, 2014, **9**, e91935.

4 X.-p. Guo, Y. Yang, D.-p. Lu, Z.-s. Niu, J.-n. Feng, Y.-r. Chen, F.-y. Tou, E. Garner, J. Xu and M. Liu, *Water Res.*, 2018, **129**, 277–286.
5 M. Abbondio, I. Fois, C. Longheu, E. Azara and S. Tola, *Small Rumin. Res.*, 2019, **174**, 83–87.
6 U. Farooq, Q. Yang, M. W. Ullah and S. Wang, *Biosens. Bioelectron.*, 2018, **118**, 204–216.
7 L. Bi, H. Zhang, W. Hu, J. Chen, Y. Wu, H. Chen, B. Li, Z. Zhang, J. Choo and L. Chen, *Biosens. Bioelectron.*, 2023, **237**, 115519.
8 G. R. Souza, D. R. Christianson, F. I. Staquicini, M. G. Ozawa, E. Y. Snyder, R. L. Sidman, J. H. Miller, W. Arap and R. Pasqualini, *Proc. Natl. Acad. Sci. U. S. A.*, 2006, **103**, 1215–1220.
9 R. T. Sturbelle, L. F. d. C. de Avila, T. B. Roos, J. L. Borchardt, O. A. Dellagostin and F. P. L. Leite, *Vet. Microbiol.*, 2015, **180**, 245–252.
10 A. Ito, A. Taniuchi, T. May, K. Kawata and S. Okabe, *Appl. Environ. Microbiol.*, 2009, **75**, 4093–4100.
11 S. Mittal, M. Sharma and U. Chaudhary, *Pathog. Global Health*, 2015, **109**, 26–29.
12 P. D. Majors, J. S. McLean, G. E. Pinchuk, J. K. Fredrickson, Y. A. Gorby, K. R. Minard and R. A. Wind, *J. Microbiol. Methods*, 2005, **62**, 337–344.
13 M. Dimopoulou, V. Kefalloniti, P. Tsakanikas, S. Papanikolaou and G.-J. E. Nychas, *Microorganisms*, 2021, **9**, 587.
14 C. Bacon, D. Hinton and T. Mitchell, *J. Appl. Microbiol.*, 2018, **125**, 867–875.
15 A. Diehl, Y. Roske, L. Ball, A. Chowdhury, M. Hiller, N. Molière, R. Kramer, D. Stöppler, C. L. Worth and B. Schlegel, *Proc. Natl. Acad. Sci. U. S. A.*, 2018, **115**, 3237–3242.
16 M. Kord, A. Ardebili, M. Jamalan, R. Jahanbakhsh, N. Behnampour and E. A. Ghaemi, *Osong Public Health Res. Perspect.*, 2018, **9**, 160.
17 G. D. Christensen, W. A. Simpson, A. L. Bisno and E. H. Beachey, *Infect. Immun.*, 1982, **37**, 318–326.
18 G. D. Christensen, W. Simpson, J. Younger, L. Baddour, F. Barrett, D. Melton and E. Beachey, *J. Clin. Microbiol.*, 1985, **22**, 996–1006.
19 K. Rebrošová, M. Šiler, O. Samek, F. Růžička, S. Bernatová, J. Ježek, P. Zemánek and V. Holá, *Food Res. Int.*, 2019, **14**, 509–517.
20 A. G. Abdelhamid, A. Esaam and M. M. Hazaa, *Saudi Pharm. J.*, 2018, **26**, 603–607.
21 L. Wang, W. Liu, J.-W. Tang, J.-J. Wang, Q.-H. Liu, P.-B. Wen, M.-M. Wang, Y.-C. Pan, B. Gu and X. Zhang, *Front. microbiol.*, 2021, **12**, 683580.
22 S. Bashir, H. Nawaz, M. I. Majeed, M. Mohsin, A. Nawaz, N. Rashid, F. Batool, S. Akbar, M. Abubakar and S. Ahmad, *Spectrochim. Acta, Part A*, 2021, **258**, 119831.
23 Y. Liu, Y.-R. Chen, X. Nou and K. Chao, *Appl. Spectrosc.*, 2007, **61**, 824–831.
24 A. Sengupta, M. Mujacic and E. J. Davis, *Anal. Bioanal. Chem.*, 2006, **386**, 1379–1386.
25 M. Fleischmann, N. Hendra and H. McQuillan, *Chem. Phys. Lett.*, 1974, **26**(2), 163–166.
26 V. Vendamani, S. N. Rao, A. P. Pathak and V. R. Soma, *ACS Appl. Nano Mater.*, 2022, **5**, 4550–4582.
27 L. Chen, B. Ying, P. Song and X. Liu, *Adv. Mater. Interfaces*, 2019, **6**, 1901346.
28 K. Wang, D.-W. Sun, H. Pu, Q. Wei and L. Huang, *ACS Appl. Mater. Interfaces*, 2019, **11**, 29177–29186.
29 L. Litti, S. Trivini, D. Ferraro and J. Reguera, *ACS Appl. Mater. Interfaces*, 2021, **13**, 34752–34761.
30 B. Zhao, H. Liu, L. Xia, Z. Wang and C. Zhang, *ACS Appl. Nano Mater.*, 2022, **5**, 15341–15352.
31 L. Martinez and L. He, *ACS Appl. Bio Mater.*, 2020, **4**, 295–310.
32 A. Tripathi and J. Bonilla-Cruz, *ACS Appl. Nano Mater.*, 2023, **6**, 5042–5074.
33 A. Fularz, S. Almohammed and J. H. Rice, *ACS Appl. Nano Mater.*, 2020, **3**, 1666–1673.
34 A. Petrovic Fabijan, R. C. Y. Lin, J. Ho, S. Maddocks, N. L. Ben Zakour, J. R. Iredell, A. Khalid, C. Venturini, R. Chard, S. Morales, I. Sandaradura, T. Gilbey and Westmead Bacteriophage Therapy, *Nat. Microbiol.*, 2020, **5**, 465–472.
35 X. Zhou, Z. Hu, D. Yang, S. Xie, Z. Jiang, R. Niessner, C. Haisch, H. Zhou and P. Sun, *Adv. Sci.*, 2020, **7**, 2001739.
36 L. Jiang, G. Niu, H. Wu, J. Zhao, Y. Liu, Z. Xie, Q. Yao, W. Yu, W. Ren and G. Zhao, *ACS Appl. Nano Mater.*, 2021, **4**, 8972–8978.
37 P. Dharmalingam, K. Venkatakrishnan and B. Tan, *ACS Appl. Mater. Interfaces*, 2022, **14**, 6370–6386.
38 Y.-F. Chen, W.-R. Chang, J.-H. Wang, C.-F. J. Kuo, C.-C. Cheng and C.-W. Chiu, *ACS Appl. Nano Mater.*, 2023, **6**, 13604–13615.
39 P. Moitra, A. Chaichi, S. M. A. Hasan, K. Dighe, M. Alafeef, A. Prasad, M. R. Gartia and D. Pan, *Biosens. Bioelectron.*, 2022, **208**, 114200.
40 S. Bashir, H. Nawaz, M. I. Majeed, M. Mohsin, S. Abdullah, S. Ali, N. Rashid, M. Kashif, F. Batool and M. Abubakar, *Photodiagn. Photodyn. Ther.*, 2021, **34**, 102280.
41 A. Mushtaq, H. Nawaz, M. I. Majeed, N. Rashid, M. Tahir, M. Z. Nawaz, K. Shahzad, G. Dastgir, R. Z. A. Bari and A. ul Haq, *Spectrochim. Acta, Part A*, 2022, **278**, 121315.
42 M. Kashif, M. I. Majeed, H. Nawaz, N. Rashid, M. Abubakar, S. Ahmad, S. Ali, H. Hyat, S. Bashir and F. Batool, *Spectrochim. Acta, Part A*, 2021, **261**, 119989.
43 H. Zhu, J. Zhang, X. Dai, V. S. D. Mesias, H. Chi, C. Wang, C. S. Yeung, Q. Chen, W. Liu and J. Huang, *Anal. Bioanal. Chem.*, 2023, 1–11.
44 M. Saleem, M. I. Majeed, H. Nawaz, M. A. Iqbal, A. Hassan, N. Rashid, M. Tahir, A. Raza, H. M. ul Hassan and A. Sabir, *Anal. Lett.*, 2022, **55**, 2132–2146.
45 X.-F. Zhang, Z.-G. Liu, W. Shen and S. Gurunathan, *Int. J. Mol. Sci.*, 2016, **17**, 1534.
46 S. Keleştemur and M. Çulha, *Appl. Spectrosc.*, 2017, **71**, 1180–1188.
47 S. Keleştemur, E. Avci and M. Çulha, *Chemosensors*, 2018, **6**, 5.
48 A. B. Beyene, W.-N. Su, H.-C. Tsai, W. A. Tegegne, C.-H. Chen, C.-C. Huang, D. Mares, V. Prajzler,

W.-H. Huang and B. J. Hwang, *ACS Appl. Nano Mater.*, 2022, **5**, 11567–11576.
49 L. Bi, X. Wang, X. Cao, L. Liu, C. Bai, Q. Zheng, J. Choo and L. Chen, *Talanta*, 2020, **220**, 121397.
50 R. A. Haque, N. Hasanudin, M. A. Iqbal, A. Ahmad, S. Hashim, A. Abdul Majid and M. B. K. Ahamed, *J. Coord. Chem.*, 2013, **66**, 3211–3228.
51 A. Raza, S. Parveen, M. I. Majeed, H. Nawaz, M. R. Javed, M. A. Iqbal, N. Rashid, M. Z. Haider, M. Z. Ali and A. Sabir, *Spectrochim. Acta, Part A*, 2023, **285**, 121903.
52 A. Naman, H. Tahseen, H. Nawaz, M. I. Majeed, A. Ali, A. Haque, M. U. Akbar, N. Mehmood, R. Nosheen and S. Nadeem, *Spectrochim. Acta, Part A*, 2024, **305**, 123414.
53 J. Guicheteau, L. Argue, D. Emge, A. Hyre, M. Jacobson and S. Christesen, *Appl. Spectrosc.*, 2008, **62**, 267–272.
54 D. Ea, E. Eg, S. Ov, S. Na, E. En, E. Av and K. In, *Bull. Russ. State Med. Univ.*, 2018, 25–32.
55 M. L. Laucks, A. Sengupta, K. Junge, E. J. Davis and B. D. Swanson, *Appl. Spectrosc.*, 2005, **59**, 1222–1228.
56 Y. Cheong, Y. Jin Kim, H. Kang, S. Choi and H. Joo Lee, *Microsc. Res. Tech.*, 2017, **80**, 177–182.
57 S. Stöckel, J. Kirchhoff, U. Neugebauer, P. Rösch and J. Popp, *J. Raman Spectrosc.*, 2016, **47**, 89–109.
58 G. D. Sockalingum, H. Lamfarraj, A. Beljebbar, P. Pina, M. Delavenne, F. Witthuhn, P. Allouch and M. Manfait, Vibrational spectroscopy as a probe to rapidly detect, identify, and characterize micro-organisms, *Biomedical Applications of Raman Spectroscopy*, SPIE, 1999, vol. 3608.
59 S. Li, P. Huang, Z. Ye, Y. Wang, W. Wang, D. Kong, J. Zhang, L. Deng and A. Dong, *J. Mater. Chem. B*, 2019, **7**, 6024–6034.
60 J. W. Chan, H. Winhold, M. H. Corzett, J. M. Ulloa, M. Cosman, R. Balhorn and T. Huser, *Cytometry, Part A*, 2007, **71**, 468–474.
61 A. Silge, R. Heinke, T. Bocklitz, C. Wiegand, U.-C. Hipler, P. Rösch and J. Popp, *Anal. Bioanal. Chem.*, 2018, **410**, 5839–5847.
62 T. J. Moritz, D. S. Taylor, C. R. Polage, D. M. Krol, S. M. Lane and J. W. Chan, *Anal. Chem.*, 2010, **82**, 2703–2710.
63 A. C. S. Talari, Z. Movasaghi, S. Rehman and I. U. Rehman, *Appl. Spectrosc. Rev.*, 2015, **50**, 46–111.
64 X.-J. Hu, Z.-X. Liu, Y.-D. Wang, X.-L. Li, J. Hu and J.-H. Lü, *Nucl. Sci. Tech.*, 2016, **27**, 56.
65 T. Kawai and S. Akira, *Nat. Immunol.*, 2010, **11**, 373–384.